Plots for A$^\sharp$ Science Case

Shiksha Pandey[1,*] and Bangalore S. Sathyaprakash[2,3]

[1] *Institute for Gravitation & the Cosmos, Department of Physics, Penn State University, University Park, PA 16802, USA*

[2] *Institute for Gravitation & the Cosmos, Department of Physics, Penn State University, University Park PA 16802, USA*

[3] *Department of Astronomy and Astrophysics, Penn State University, University Park PA 16802, USA*

(Dated: May 29, 2025)

SENSITIVITY CURVES

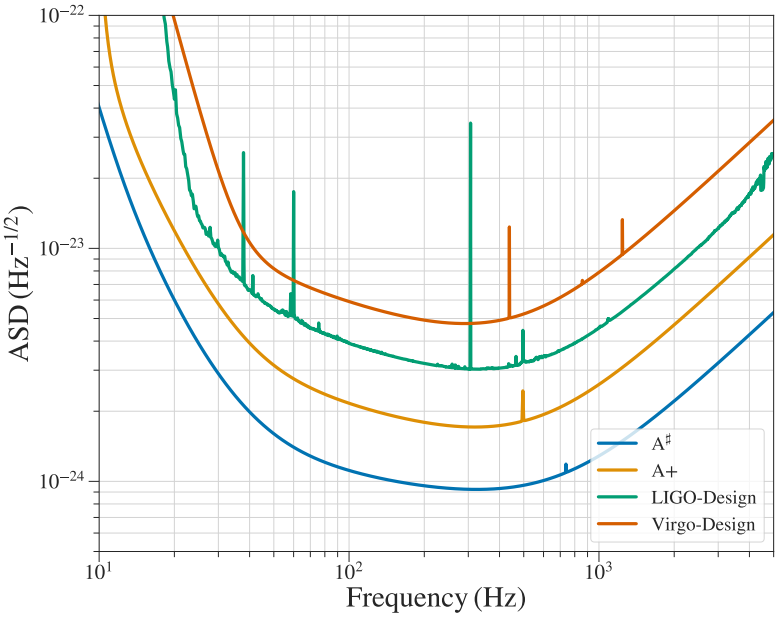

FIG. 1. Noise amplitude spectral density (ASD) curves for gravitational wave detector configurations considered, including LIGO at A$^\sharp$ [1], A+ [2] and design sensitivity [3], and Virgo at design sensitivity [3].

BINARY NEUTRON STAR (BNS) MERGERS

For the binary neutron star (BNS) population, we adopt the following parameters:

- **Mass Distribution:** A double Gaussian model is used:

$$p(m) = wN(\mu_L, \sigma_L) + (1-w)N(\mu_R, \sigma_R),$$

where the mean and standard deviation for the lower peak are $\mu_L = 1.35M_\odot$ and $\sigma_L = 0.08M_\odot$, and for the higher peak are $\mu_R = 1.8M_\odot$ and $\sigma_R = 0.3M_\odot$, and the relative weight of the lower peak is $w = 0.64$ [4]. The distribution is truncated to $[1, 2.2]M_\odot$.

- **Spin Properties:** The neutron stars are assumed to have low spins, with spin magnitudes uniformly distributed between $[0, 0.1]$.
- **Merger rate:** The merger rate follows a Madau-Dickinson star formation rate [5]:

$$\psi(z) = (1+z)^\gamma \left[1 + \left(\frac{1+z}{1+z_p}\right)^\kappa\right]^{-1}, \tag{1}$$

with $z_p = 1.9$, $\gamma = 2.7$, and $\kappa = 5.6$. The local merger rate density is chosen to be $105.5^{+190.2}_{-83.9}\mathrm{Gpc}^{-3}\mathrm{yr}^{-1}$ [6].

- **Equation of State (EOS):** APR4 [7] is adopted as the equation of state, consistent with the maximum mass allowed for neutron stars.
- **Waveform Model:** Gravitational wave signals are generated using IMRPhenomPv2_NRTidalv2 [8] waveform model.

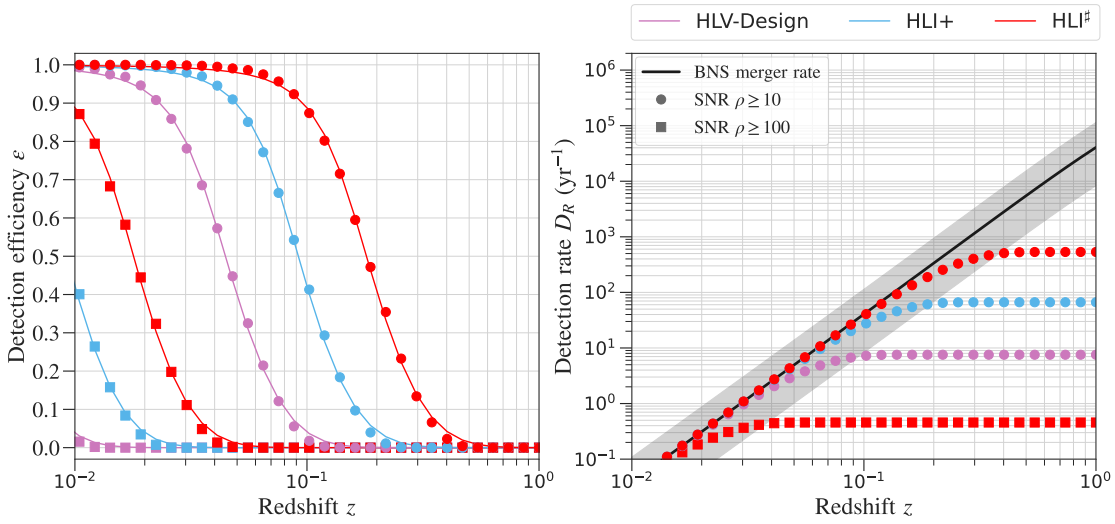

FIG. 2. Detection efficiency and detection rate as functions of redshift for three detector networks, evaluated using threshold signal-to-noise ratios (SNRs) of 10 (circles) and 100 (squares). In the right panel, the solid black line represents the cosmic binary neutron star merger rate, while the grey-shaded region illustrates the variation in merger rate due to uncertainties in the local merger rate density.

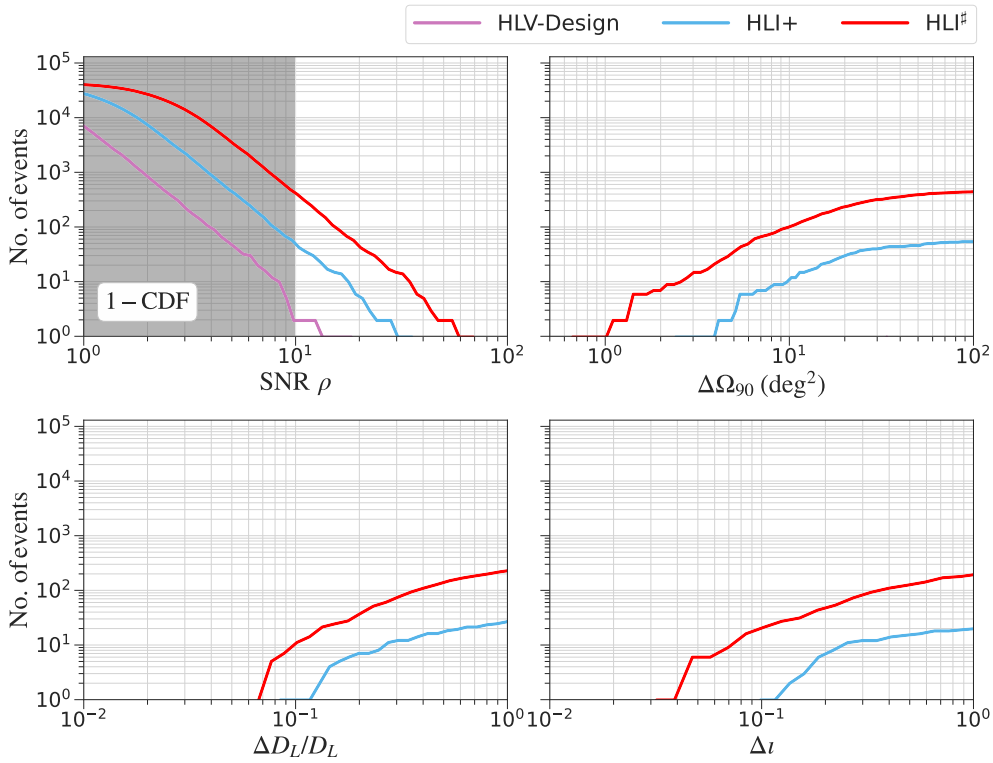

FIG. 3. Scaled cumulative distribution of binary neutron star merger events per year as a function of signal-to-noise ratio (SNR), 90% credible source localization area ($\Delta\Omega_{90}$), relative uncertainty in luminosity distance ($\Delta D_L/D_L$), and uncertainty in inclination angle ($\Delta\iota$), where the uncertainties are quoted at 68% credible interval. In the top-left panel, the gray-shaded region highlights events with SNRs below the typical detectability threshold of 10.

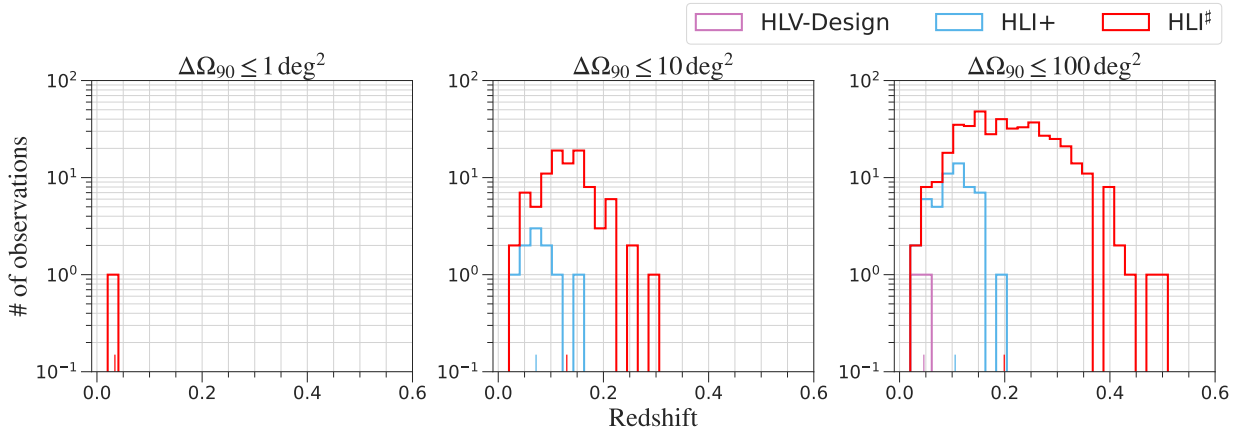

FIG. 4. Annual binary neutron star merger observations with respect to redshift for three 90% credible source localization areas ($\Delta\Omega_{90}$): ≤ 1 deg^2 (left), ≤ 10 deg^2 (center), ≤ 100 deg^2 (right). The distributions illustrate the redshift reach of three gravitational wave detector networks for precise source localization.

TABLE I. The annual count of BNS mergers and the median and maximum redshift (up to z = 1) for detected events corresponding to specific $\Delta\Omega_{90}$. These figures are based on the median local merger rates for BNS = 105.5 $\mathrm{Gpc^{-3}yr^{-1}}$.

Quantity	HLV-Design	HLI+	HLI$^\sharp$
$\Delta\Omega \leq 1$ deg^2			
Number	0	0	1
Median z	-	-	0.034
Maximum z	-	-	0.034
$\Delta\Omega \leq 10$ deg^2			
Number	0	10	97
Median z	-	0.072	0.13
Maximum z	-	0.151	0.299
$\Delta\Omega \leq 100$ deg^2			
Number	2	54	435
Median z	0.046	0.106	0.199
Maximum z	0.058	0.185	0.495

BINARY BLACK HOLE (BBH) MERGERS

The binary black hole (BBH) population is modeled with the following specifications:

- **Mass Distribution:**
  - The primary mass follows the POWER LAW + PEAK model [6]:

    $$p(m_1) \propto m_1^{\alpha},$$

    with parameters $\alpha = -3.4$, $m_{\mathrm{min}} = 5M_\odot$, $m_{\mathrm{max}} = 87M_\odot$, $\lambda = 0.04$, $\mu_{\mathrm{peak}} = 34M_\odot$, $\sigma_{\mathrm{peak}} = 3.6M_\odot$, and $\delta m = 4.8M_\odot$.
  - The mass ratio $q = m_2/m_1$ follows $p(q) \propto q^{\beta}$, where $\beta = 1.1$.
- **Spin Properties:** The spin magnitudes of black holes, restricted to alignment with the orbital angular momentum, follow a beta distribution [9]:

  $$p(\chi_i \mid \alpha_{\chi_i}, \beta_{\chi_i}) = \frac{\chi_i^{\alpha_{\chi_i}-1}(\chi_{\mathrm{max}} - \chi_i)^{\beta_{\chi_i}-1}}{\mathrm{B}(\alpha_{\chi_i}, \beta_{\chi_i})\chi_{\mathrm{max}}^{\beta_{\chi_i}+\alpha_{\chi_i}-1}},$$

  where χ_i is the spin magnitude in $[0, \chi_{\mathrm{max}} = 1]$, and $\mathrm{B}(\alpha_{\chi_i}, \beta_{\chi_i})$ is the beta function. This restriction excludes precession effects while modeling spins aligned with the orbital angular momentum.
- **Merger rate:** Same as the BNS population, but with the local merger rate density = $23.9^{+14.3}_{-8.6}\,\mathrm{Gpc^{-3}\,yr^{-1}}$ [10].
- **Waveform Model:** IMRPhenomXHM waveform model was used [11].

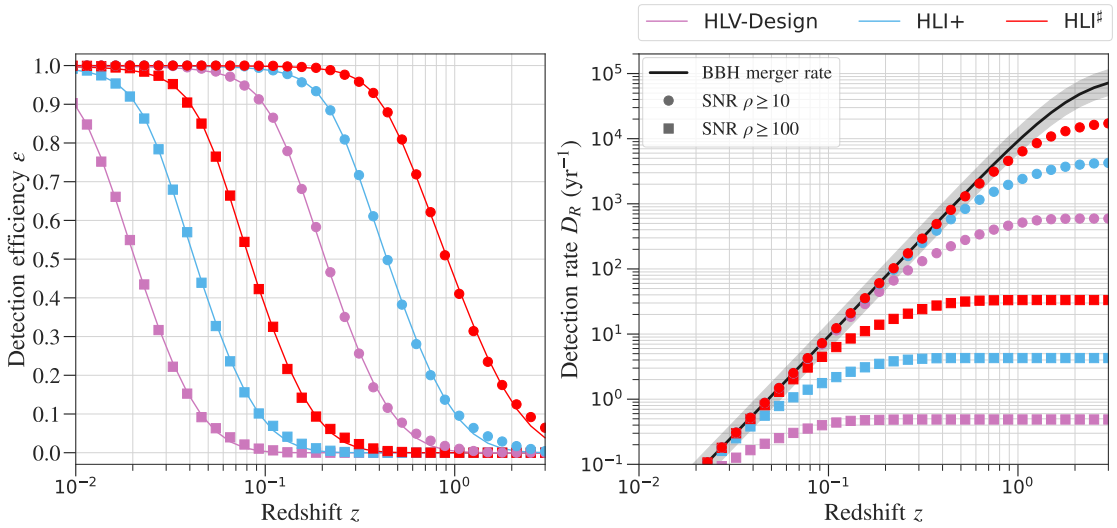

FIG. 5. Detection efficiency and detection rate as functions of redshift for three detector networks, evaluated using threshold signal-to-noise ratios (SNRs) of 10 (circles) and 100 (squares). In the right panel, the solid black line represents the cosmic black hole merger rate, while the grey-shaded region illustrates the variation in merger rate due to uncertainties in the local merger rate density.

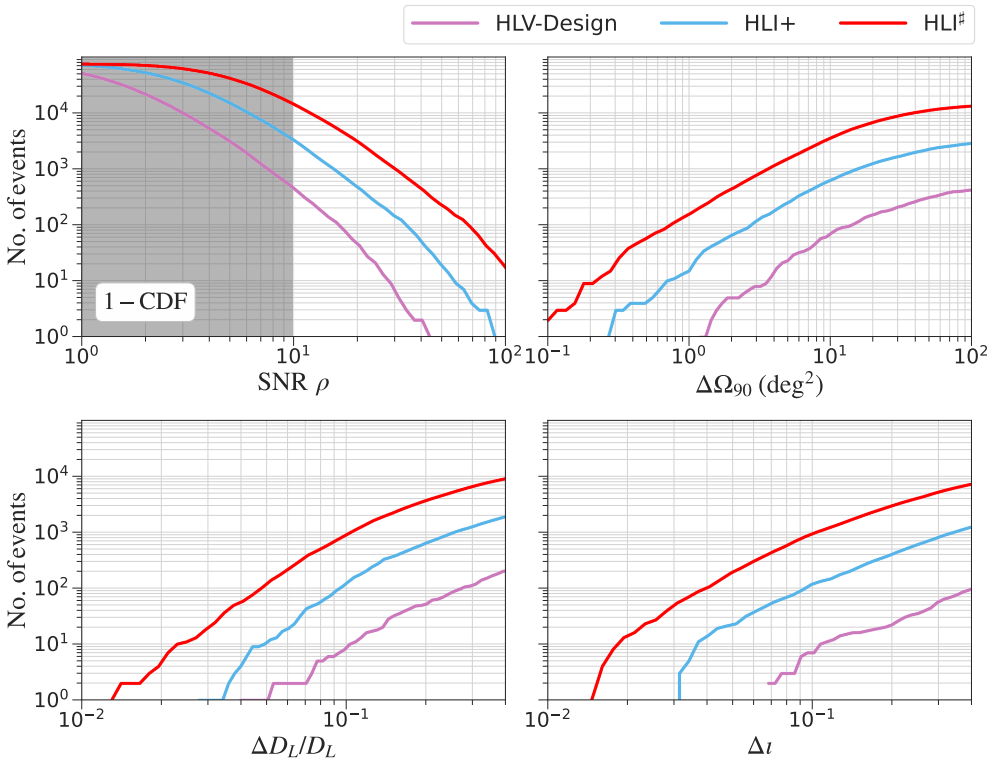

FIG. 6. Scaled cumulative distribution of black hole mergers per year as a function of signal-to-noise ratio (SNR), 90% credible source localization area ($\Delta\Omega_{90}$), relative uncertainty in luminosity distance ($\Delta D_L/D_L$), and uncertainty in inclination angle ($\Delta\iota$), where the uncertainties are quoted at 68% credible interval. In the top-left panel, the gray-shaded region highlights events with SNRs below the typical detectability threshold of 10.

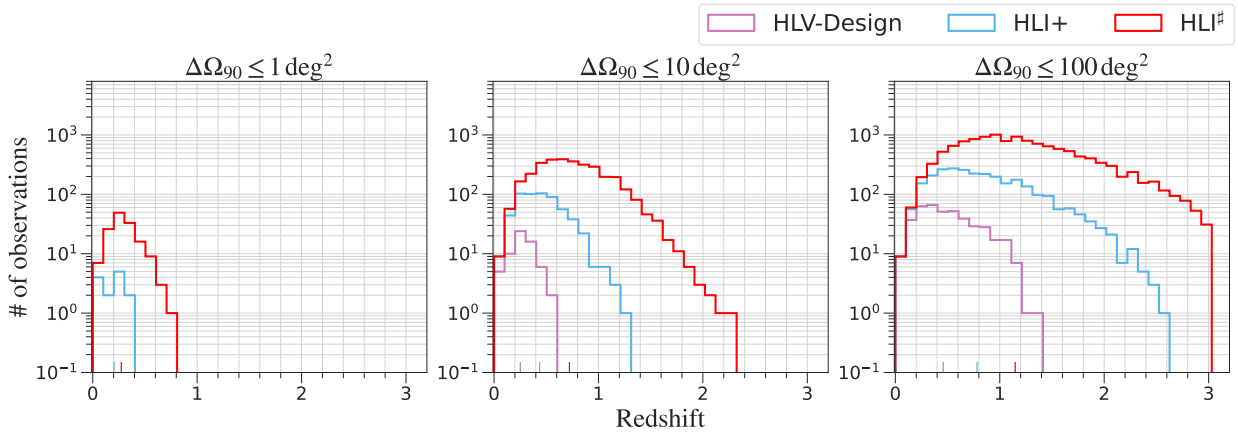

FIG. 7. Annual black hole merger observations with respect to redshift for three 90% credible source localization areas ($\Delta\Omega_{90}$): $\leq$ 1 deg^2 (left), $\leq$ 10 deg^2 (center), $\leq$ 100 deg^2 (right). The distributions illustrate the redshift reach of three gravitational wave detector networks for precise source localization.

TABLE II. The annual count of BBH mergers and the median and maximum redshift (up to z = 3) for detected events corresponding to specific $\Delta\Omega_{90}$. These figures are based on the median local merger rates for BBH = 23.9 Gpc^{-3}yr^{-1}.

Quantity	HLV-Design	HLI+	HLI♯
$\Delta\Omega \leq 1$ deg^2			
Number	0	13	144
Median z	-	0.204	0.273
Maximum z	-	0.318	0.709
$\Delta\Omega \leq 10$ deg^2			
Number	63	583	3250
Median z	0.252	0.437	0.722
Maximum z	0.592	1.294	2.288
$\Delta\Omega \leq 100$ deg^2			
Number	417	2791	12950
Median z	0.458	0.782	1.148
Maximum z	1.412	2.554	2.999

NEUTRON STAR BLACK HOLE (NSBH) MERGERS

For neutron star black hole (NSBH) population, we adopt the following parameters:

- **Mass Distribution:**
  - **Black Hole Mass:** The black hole masses follow the POWER LAW + PEAK distribution, consistent with the primary mass distribution of the local BBH population.
  - **Neutron Star Mass:** Neutron star masses are uniformly distributed in the range $[1, 2.2]M_\odot$.
- **Spin Properties:**

  - **Black Hole Spin:** Spins are assumed to be aligned with the orbital angular momentum and follow a Gaussian distribution with $\mu = 0$ and $\sigma = 0.2$.
  - **Neutron Star Spin:** Spins are assumed to be low, uniformly distributed in the range $[-0.1, 0.1]$.

- **Redshift Distribution:** The redshift follows the same Madau-Dickinson star formation rate as BNSs and BBHs. The local merger rate density is set to $45^{+75}_{-33}\,\mathrm{Gpc}^{-3}\,\mathrm{yr}^{-1}$.

- **Waveform Model:** Same as BBH.

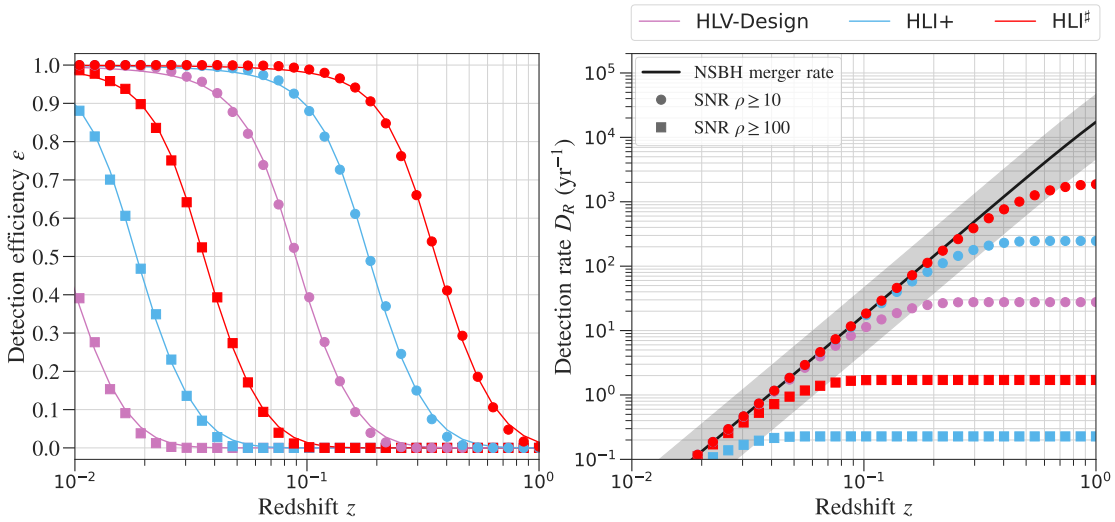

FIG. 8. Detection efficiency and detection rate as functions of redshift for three detector networks, evaluated using threshold signal-to-noise ratios (SNRs) of 10 (circles) and 100 (squares). In the right panel, the solid black line represents the cosmic neutron star black hole merger rate, while the grey-shaded region illustrates the variation in merger rate due to uncertainties in the local merger rate density.

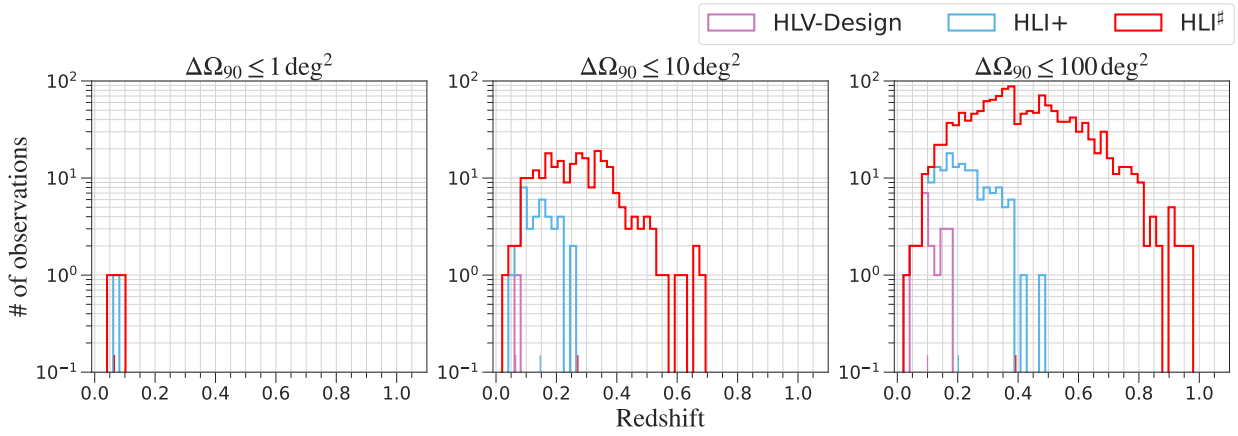

FIG. 9. Annual neutron star black hole merger observations with respect to redshift for three 90% credible source localization areas ($\Delta\Omega_{90}$): ≤ 1 deg^2 (left), ≤ 10 deg^2 (center), ≤ 100 deg^2 (right). The distributions illustrate the redshift reach of three gravitational wave detector networks for precise source localization.

TABLE III. The annual count of NSBH mergers and the median and maximum redshift (up to z = 1) for detected events corresponding to specific $\Delta\Omega_{90}$. These figures are based on the median local merger rates for NSBH = 45 $\mathrm{Gpc^{-3}yr^{-1}}$.

Quantity	HLV-Design	HLI+	HLI$^\sharp$
$\Delta\Omega \leq 1$ deg^2			
Number	0	1	3
Median z	-	0.065	0.065
Maximum z	-	0.065	0.099
$\Delta\Omega \leq 10$ deg^2			
Number	1	37	241
Median z	0.065	0.146	0.271
Maximum z	0.065	0.261	0.681
$\Delta\Omega \leq 100$ deg^2			
Number	20	161	1397
Median z	0.1	0.202	0.392
Maximum z	0.182	0.479	0.977

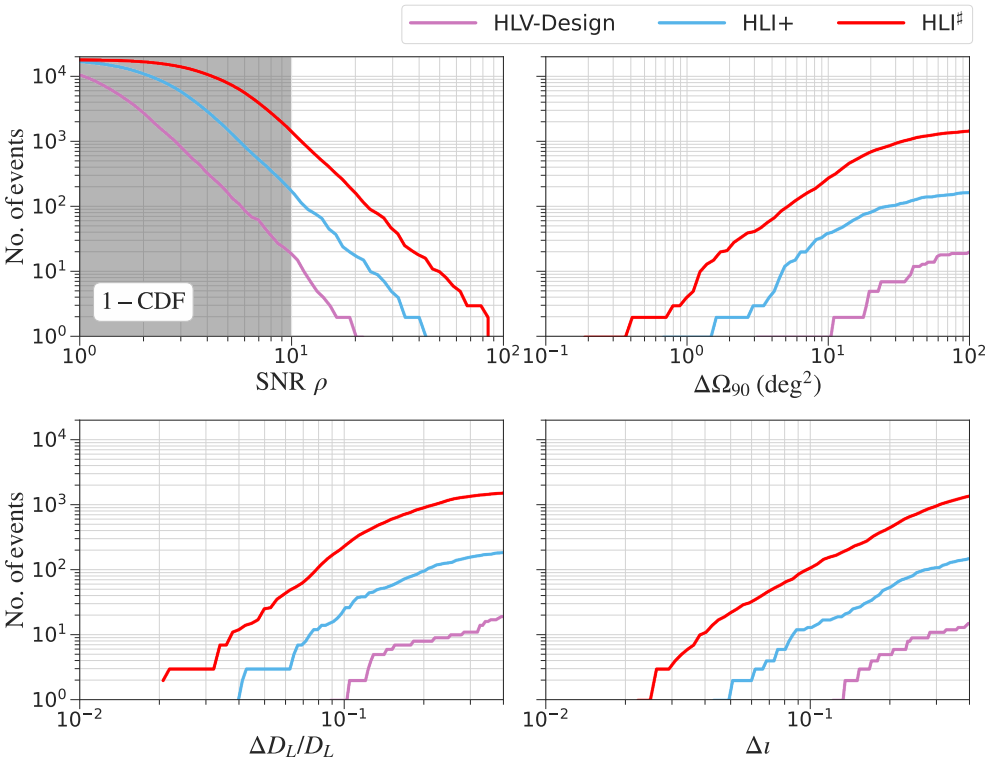

FIG. 10. Scaled cumulative distribution of neutron star black hole mergers per year as a function of signal-to-noise ratio (SNR), 90% credible source localization area ($\Delta\Omega_{90}$), relative uncertainty in luminosity distance ($\Delta D_L/D_L$), and uncertainty in inclination angle ($\Delta\iota$), where the uncertainties are quoted at 68% credible interval. In the top-left panel, the gray-shaded region highlights events with SNRs below the typical detectability threshold of 10.

* spp5950@psu.edu

[1] L. S. Collaboration, *A# Sensitivity Curve: Instrument Science White Paper 2023*, Tech. Rep. LIGO-T2300041 (LIGO Document Control Center, 2023).
[2] C. E. Collaboration, *Cosmic Explorer: The Next-Generation Gravitational-Wave Observatory*, Tech. Rep. CE-T2000007 (Cosmic Explorer Project Office, 2020).
[3] L. S. Collaboration, *Instrument Science White Paper 2022*, Tech. Rep. LIGO-T2200043 (LIGO Document Control Center, 2022).
[4] W. M. Farr and K. Chatziioannou, A population-informed mass estimate for pulsar j0740+6620, Research Notes of the AAS **4**, 65 (2020).
[5] P. Madau and M. Dickinson, Cosmic star-formation history, Annual Review of Astronomy and Astrophysics **52**, 415–486 (2014).
[6] R. Abbott *et al.*, The population of merging compact binaries inferred using gravitational waves through gwtc-3 (2022), arXiv:2111.03634 [astro-ph.HE].
[7] A. Akmal, V. R. Pandharipande, and D. G. Ravenhall, Equation of state of nucleon matter and neutron star structure, Physical Review C **58**, 1804–1828 (1998).
[8] T. Dietrich, A. Samajdar, S. Khan, N. K. Johnson-McDaniel, R. Dudi, and W. Tichy, Improving the nrtidal model for binary neutron star systems, Physical Review D **100**, 10.1103/physrevd.100.044003 (2019).
[9] D. Wysocki, J. Lange, and R. O'Shaughnessy, Reconstructing phenomenological distributions of compact binaries via gravitational wave observations, Physical Review D **100**, 10.1103/physrevd.100.043012 (2019).
[10] R. Abbott *et al.* (The LIGO Scientific Collaboration, The Virgo Collaboration), Population properties of compact objects from the second ligo–virgo gravitational-wave transient catalog, The Astrophysical Journal Letters **913**, L7 (2021).
[11] C. García-Quirós, M. Colleoni, S. Husa, H. Estellés, G. Pratten, A. Ramos-Buades, M. Mateu-Lucena, and R. Jaume, Multimode frequency-domain model for the gravitational wave signal from nonprecessing black-hole binaries, Physical Review D **102**, 10.1103/physrevd.102.064002 (2020).